J Mater Sci (2011) 46:6563–6570
DOI 10.1007/s10853-011-5603-8

Electrical and tribological properties of a Ni–18%Ru alloy for contact applications

Y. Liu · B. S. Senturk · J. V. Mantese · M. Aindow · S. P. Alpay

Received: 20 January 2011 / Accepted: 2 May 2011 / Published online: 12 May 2011

Abstract A study of the microstructure, development of contact resistance during oxidation, and abrasive wear behavior for a Ni–18 at.%Ru alloy is presented in this article. It is shown that the alloy can be solutionized and aged, resulting in a fine lamellar mixture of FCC α-Ni and HCP β-Ru phases. Upon oxidation in air for 400 h, the measured contact resistance of the alloy is two orders of magnitude lower than that of pure Ni after 400-h oxidation. This behavior results from the formation of a low-resistivity rutile RuO_2 scale on the β phase lamellae, which gives conducting pathways through the insulating NiO scale that forms on the α phase. After an initial run-in period, the steady-state abrasive wear rate measured for the Ni–Ru alloy is an order of magnitude less than that of pure Ni. Since the micro-cutting and flaking wear mechanisms are the same, the differences in the wear rates are ascribed to the presence of the well-dispersed hard Ru-rich β phase. The combination of a low-resistivity self-healing native oxide scale and good wear properties makes the alloy an excellent candidate for electrical contact applications.

Introduction

Electrical contacts that connect electrical and electronic components/systems can be found in almost every technological application, including all electronic devices and telecommunication systems. The selection of high-reliability materials for the full range of residential, commercial, and aerospace applications poses formidable challenges to the connection system designer. Since approximately one trillion electrical contacts are produced annually, it is highly preferable that the materials for the production of contacts should be both inexpensive and readily formable [1–3]. As such, base metals are the materials of choice for electrical contacts. Unfortunately, base metals such as Cu and Al oxidize in air under ambient conditions. The native oxide scales of these metals (Cu_2O/CuO on Cu and Al_2O_3 on Al) result in contact resistances that are orders of magnitude higher than those for mating bare metal surfaces [2, 3]. The development of unacceptably high contact resistances over time is by far the most common cause of failure in electronic devices and systems [3].

A common solution to this problem is to coat the contact with a thin layer of a different metal. For low-cost applications, the second metal is typically Sn which forms a thin soft passivating SnO_2 scale in air; although the resistivity of SnO_2 is high, the scale is easily removed by abrasion when forming the electrical connection. Noble metals such as Au, Ag, Pd, or Pt are used for more critical applications where the improved reliability of the contact outweighs the penalty of added cost. While such coatings can be applied readily by electroplating, this adds significantly to production costs, and there are undesirable environmental impacts associated with most of the electrolyte formulations used in such processes [1–3]. Furthermore, coatings are easily ruptured and displaced when a force is applied by the mating contact surfaces. Over time, high-resistivity wear debris accumulates between the mating surfaces of the contacts, eventually causing failure. In view of the

Y. Liu · B. S. Senturk · M. Aindow · S. P. Alpay (✉)
Department of Chemical Materials and Biomolecular Engineering and Institute of Materials Science, University of Connecticut, Storrs, CT 06269, USA
e-mail: p.alpay@ims.uconn.edu

J. V. Mantese
United Technologies Research Center, East Hartford, CT 06108, USA

above, the use of plated contacts does not eliminate problems resulting from abrasive wear and/or fretting; these processes can compromise the integrity of the coating, exposing the bare base metal, and allowing a highly resistive scale to develop [4–6].

In a recent study, we have approached this problem by developing strategies for alloying base metals to promote the formation of inherently conductive native oxide scales [7]. The use of such alloys for electrical contacts would eliminate the need for plating and, since the native scales would be electrically self-healing, contacts produced from these alloys would be far more reliable in situations where abrasive wear or fretting might occur. We have previously identified several distinct approaches for enhancing the conductivity of oxide scales [7]. These include doping to increase mobile carrier concentration, inducing mixed oxidation states resulting in electron/polaron hopping, and phase separation giving conducting pathways.

The example given previously [7] for a system in which the phase separation approach could be exploited was a peritectic Ni–Ru alloy where the components are essentially immiscible at ambient temperatures (Fig. 1a). Thus, the microstructures of Ni–Ru alloys with Ru concentrations of less than 30 at.% should consist of Ru-rich dendrites/particles in a Ni-rich matrix. The oxides NiO and RuO_2 are also immiscible (Fig. 1b), and RuO_2 is an excellent metallic conductor [8–11]. Indeed, our previous findings [7] show that the contact resistance values for the oxidized Ni–28 at.%Ru (Ni–28Ru) samples are lower than those for high-purity Ni samples for all oxidation times at 100 °C in air, and after 400-h oxidation, the discrepancy is two to three orders of magnitude (Fig. 2). Figure 2 also shows contact resistance values obtained from pure Cu under the same conditions, and these are fully over six orders of magnitude higher than those of the Ni–28Ru after extended exposures (>100 h). We have ascribed the improvement in the contact resistance on alloying Ni with Ru to the formation of RuO_2 that serves as conducting pathways through the more resistive NiO phase [7, 11–14]. Although the bulk resistivity of this alloy is somewhat higher than that of pure Ni (621.0 nΩ m c.f. 67.2 nΩ m [7]), this value is within acceptable limits for contact applications [3].

While the properties of the Ni–28Ru alloy are promising for contact applications, there are two factors that might limit the exploitation of this alloy. First, Ru is a fairly expensive metal, and thus the high Ru content might make the cost of this alloy prohibitive for the majority of applications. Second, the single α-phase field only extends from 1360 to 1450 °C at this composition (Fig. 1a), and this may present an unreasonably narrow processing window for the alloy. Both of these issues would be addressed partly if the Ru content of the alloy could be reduced without compromising the electrical properties unduly. To this end, we

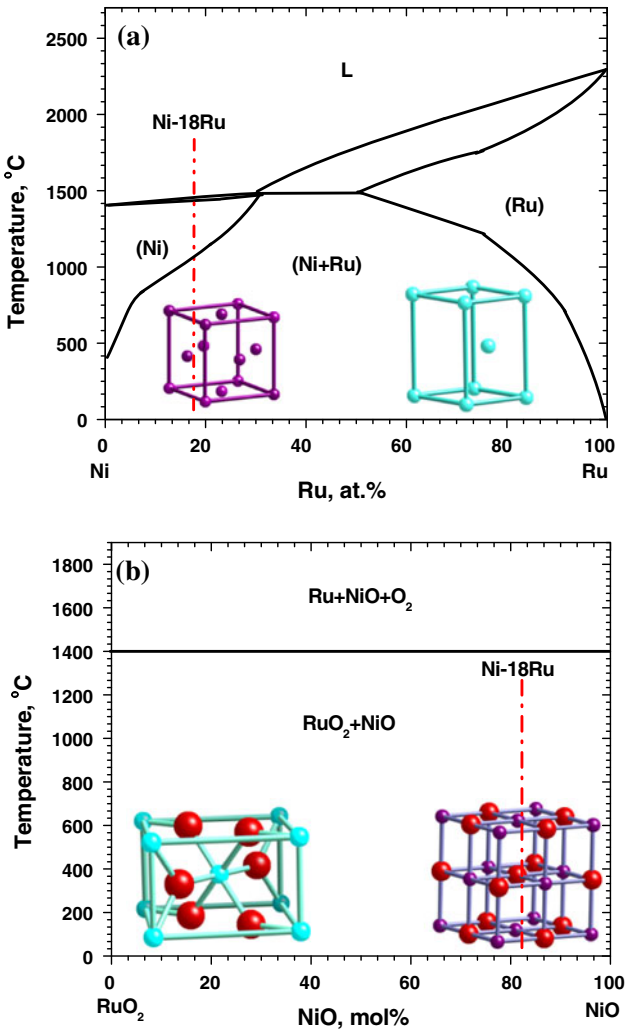

Fig. 1 Equilibrium **a** Ni–Ru and **b** RuO_2–NiO phase diagrams. The *dashed lines* in **a**, **b** show the composition of the alloys used in this study. Also shown on both diagrams are the crystal structures of the end components

present here a study on the microstructure, contact resistance, and wear properties of a Ni–18 at.% Ru (Ni–18Ru) alloy. This alloy contains fully 1/3 less Ru than the Ni–28Ru composition considered previously [7], and has a single α-phase field that extends from 1080 to 1430 °C. It is shown that the contact resistance of the alloy is comparable to that of the Ni–28Ru and that the wear properties are far superior to those of both pure Ni and pure Cu.

Experimental

The Ni–18Ru alloy was produced from high-purity elemental starting materials by an arc-melting process in an argon-shielded chamber. The alloy ingot was melted five times to obtain a homogeneous microstructure. After the final melting stage, the alloy was cast into cylindrical

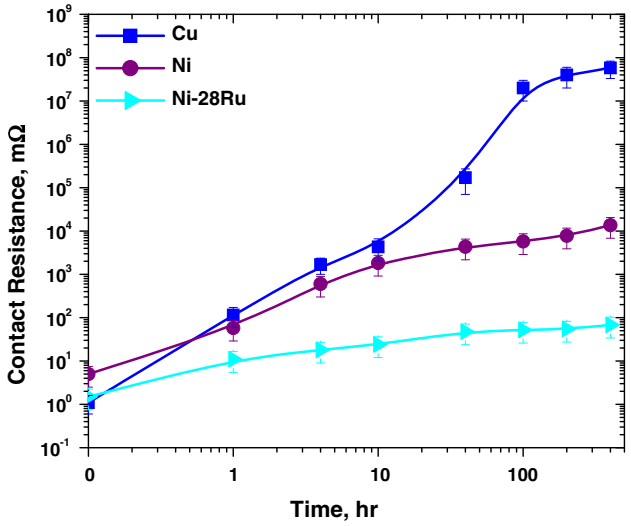

Fig. 2 Contact resistance of Ni–28Ru alloys oxidized at 100 °C as a function of oxidation time. Also shown are the contact resistance values obtained from pure Cu and pure Ni under the same conditions. Adapted from Ref. [7]. The *error bars* are $\pm 0.5\ \sigma$, where σ is the standard deviation of the measurements. The lines through the data are schematic trend lines drawn to help guide the eye

ingots 25 mm in diameter. Samples for subsequent experiments were obtained by slicing disks of ~6 mm in thickness from these ingots. The samples were subsequently heat treated by encapsulating in evacuated quartz glass tubes back-filled with Ar, homogenizing at 1100°C for 4 days, quenching into water, and then aging at 600°C for 20 h to precipitate the Ru-rich β phase.

The microstructure and chemistry of the alloy, and the oxide film were characterized using a combination of X-ray Diffraction (XRD), Scanning Electron Microscopy (SEM), and Transmission Electron Microscopy (TEM). The XRD analyses were performed using a Bruker D5005 Diffractometer; for the unoxidized alloy, conventional Bragg-Bretano θ–2θ scans were obtained, while for the oxidized samples the data were obtained using the X-ray beam at glancing incidence (0.5°–1°) to enhance the signal from the thin oxide scale. Metallographic samples of the alloy were prepared by mechanical polishing, followed by etching in waterless Kalling's solution for 10–15 s to reveal the microstructure. These samples were examined in a JEOL JSM-6335F field emission (FE) SEM equipped with a Thermo Noran System Six energy-dispersive X-ray spectrometer (EDXS) and operating at an accelerating voltage of 15 kV. The TEM experiments were performed in an FEI Tecnai T12 TEM, equipped with an EDAX r-TEM EDXS and operating at an accelerating voltage of 120 kV. Thin foils for TEM were prepared by twin-jet electropolishing to perforation using a solution consisting of 70% butanol, 20% perchloric acid, and 10% ethanol. The samples were then ion-milled using the cold stage of a Gatan Duomill 600 to reduce differential thinning effects from the electropolishing process. To avoid specimen preparation artifacts, TEM samples were not produced from the oxidized alloy disks, instead thin foil alloy samples were oxidized under the same conditions as those used for the oxidation experiments described below, and these oxidized thin foils were then examined directly in the TEM.

The bulk resistivity of the alloy was measured using the 2-point 4-probe method with a Keithley 2100 current meter as the source, and using an Agilent 34401A multimeter to record the voltage drop. Strip samples with dimensions of $1 \times 1 \times 20$ mm were cut from the alloy and these strips were polished to an 800 grit finish to remove any oxide before the measurements. The current was varied from 0.1 to 1 A, and the electrode position was varied three times for each sample. The resistivity of the alloy was obtained by averaging six different measurements. For contact resistance measurements, 6-mm-thick disk samples were polished mechanically to a ~1-μm finish, and then oxidized at 100 °C in air using a muffle furnace with a temperature-control of ±3 °C. The integrity of the contact surface was monitored by measuring the development of the contact resistance as a function of oxidation time, following ASTM standard B667-97 [15]. A probe with a hemispherical gold-coated end (3-mm radius) was applied to the oxidized surface with a contact load of 0.25 N as measured using a load cell. To avoid dielectric breakdown of the oxide scale, the current input was monitored carefully to ensure that this remained within the range from 1 pA to 10 nA. For each oxidation time interval, 8–10 measurements were conducted at various locations on the sample, and in each case, the mean value of the measured values was reported along with the standard deviation.

Abrasive wear resistance tests were conducted using a Struer Roto Force-4 polisher. This involves the sliding of cylindrical coupons (25 mm in diameter) against a 120-grit SiC paper, which is fixed on a static mating disk. The load is 5 N and the sliding is unidirectional under dry wear conditions (i.e., without lubricants). The test sample was rotated at 150 rpm, which corresponds to a relative sliding speed between the coupons and the mating disk of ~0.67 m/s. The mass losses of the Ni–18Ru alloy samples and reference samples of pure Cu and Ni were measured with a 0.1 mg accuracy after 2.5, 5, 10, and 20 min of sliding for each sample. Upon removal from the sliding wear apparatus, the position of the sample was marked, and the sample was returned to the same location after mass measurements. Four samples were tested for each material, and the mean value of the measured mass loss was reported along with the standard deviation of the data. Before each such measurement, the samples were cleaned ultrasonically in ethanol and then dried in flowing cool air to prevent oxidation.

Results and discussion

Microstructure of the alloy and the oxide scale

The as-cast Ni–18Ru alloy exhibited a coarse, cored dendritic α/β microstructure similar to that observed previously for Ni–28Ru [7]. The heat-treatment sequence described in the "Experimental" Section was designed to produce a finer, more homogeneous microstructure suitable for electrical contact applications (i.e., giving reproducible contact properties). After quenching from the homogenization temperature (1100 °C), the alloy exhibited a coarse-grained (>100 μm) single-phase α microstructure as revealed by XRD and SEM. For brevity, we present here only the data obtained from the alloy after aging this supersaturated solid solution at 600 °C for 20 h.

Examples of the XRD data obtained from the heat-treated Ni–18Ru alloy before and after oxidation at 100 °C for 400 h are shown in Fig. 3a, b, respectively. All of the peaks present in Fig. 3a correspond to those for the Ni-rich FCC α phase and the Ru-rich HCP β phase, as expected from the equilibrium Ni–Ru phase diagram (Fig. 1a). Similarly, the additional peaks present in Fig. 3b can all be ascribed to the equilibrium cubic NaCl-type NiO, and tetragonal rutile RuO_2 phases anticipated on the basis of the oxide phase diagram (Fig. 1b).

The distribution of these phases can be seen clearly in SEM images from the metallographic samples such as those shown in Fig. 4. The unoxidized sample was comprised entirely of large (>100 μm) colonies of parallel lamellae, and the thicknesses of the individual layers were in the range of 0.10–0.25 μm. This is consistent with the precipitation of the β phase from the supersaturated α during heat treatment via a cooperative growth process from a limited number of preferential nucleation sites. It is tempting to speculate that these sites correspond to the prior grain boundaries in the supersaturated α phase, but further work is required to confirm this. In EDXS data obtained from these surfaces, the protruding lamellae are Ni-rich, whereas the recessed regions are Ru-rich indicating that the Kalling's etchant used to prepare these samples attacks the β phase preferentially. The lamellar morphology of the underlying alloy is replicated in the surface topography of the oxidized alloy samples as observed in secondary electron SEM images, Fig. 4b. In such images, the Ru-rich regions protrude from the surface; this could indicate a higher oxidation rate for the β phase, although we note that the Pilling–Bedworth ratio will be somewhat higher for the formation of rutile RuO_2 from the β phase than for NaCl-type NiO from the α phase, and so the observed topography could develop even if the oxidation rates for the two phases were the same.

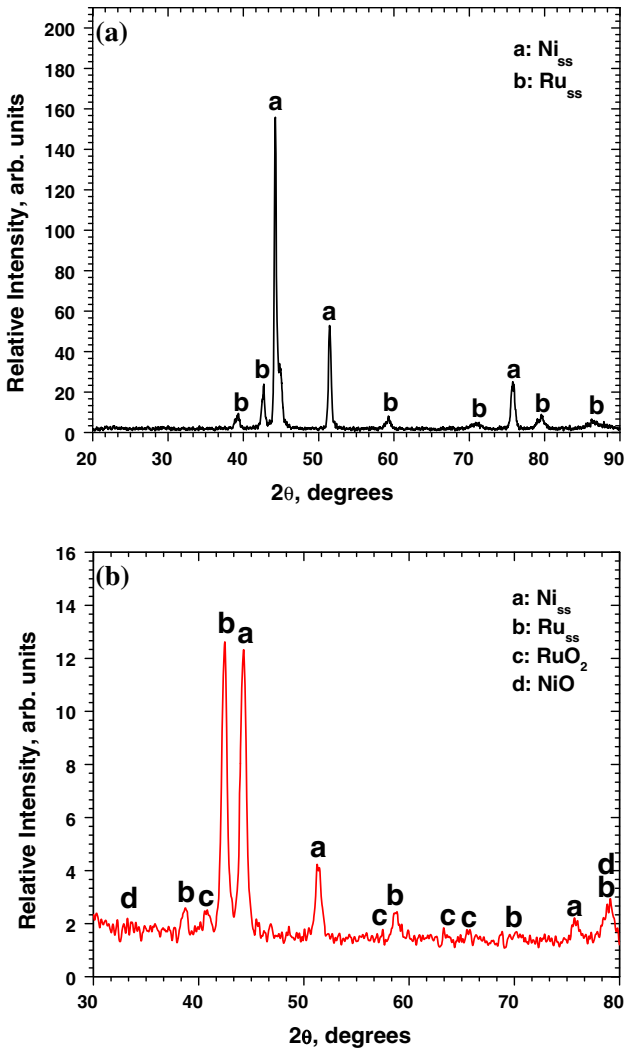

Fig. 3 The XRD data obtained from samples of the heat-treated Ni–18Ru alloy: **a** scan in Bragg-Bretano geometry from an unoxidized sample showing the presence of the Ni-rich FCC α phase and the Ru-rich HCP β phase; **b** data obtained at glancing incidence (0.5°–1.0°) from a Ni–18Ru alloy oxidized at 100 °C in air for 400 h showing the presence of both NiO and RuO_2 phases

The TEM observations provide additional insights into the form of these oxides. Figure 5a is a representative bright field TEM image of an alloy foil oxidized for 40 h at 100 °C. Under these conditions, the oxide thickness is significantly less than that of the foil, and thus the contrast is dominated by the characteristics of the underlying alloy. In the image shown, the minority β phase appears dark due to mass-thickness contrast, and the dimensions of the lamellae are consistent with those expected on the basis of the SEM observations (Fig. 4a). Figure 5b is a selected area diffraction pattern (SADP) obtained from the region shown in Fig. 5a. The pattern comprises mainly discrete spots, indicating that the region consists of a small number of large grains. From the spacings of these spots, it was

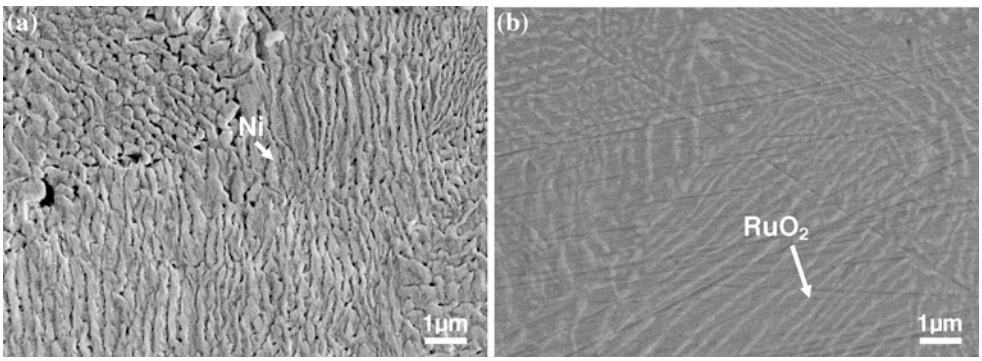

Fig. 4 : Secondary electron SEM images obtained from samples of the heat-treated Ni–18Ru alloy: **a** etched metallographic section from an unoxidized sample showing a lamellar structure made up of the Ni-rich α phase and the Ru-rich β phase; **b** polished sample oxidized at 100 °C in air showing that the lamellar morphology of the underlying alloy is replicated in the surface topography of the oxide scale

found that four crystalline phases (α-Ni, β-Ru, NiO and RuO_2) were present; while all of the spots have been indexed as belonging to these phases, it is not possible to represent these clearly and, instead, a few examples of the indices are shown on Fig. 5b. Since the diffraction maxima from both the NiO and the RuO_2 phases are discrete spots rather than continuous rings, we infer that the oxides must form epitaxially on the corresponding phases rather than as fine-grained polycrystalline scales as observed for our other candidate alloys [7]. This is consistent with the SADP data that were obtained previously from the Ni–28Ru alloy.

Electrical properties

The bulk resistivity measured from the heat-treated Ni–18Ru alloy was 450.1 nΩ m, which is within the normal range for contact applications (10^{-8} to 10^{-6} Ωm) and is somewhat lower than the value of 621.0 nΩ m obtained previously for Ni–28Ru [7]. The difference between the values for the Ni–18Ru and Ni–28Ru alloys is presumably related to the large differences in the bulk conductivities of Ni and Ru. Thus, since the volume fraction of the Ru-rich β phase in Ni–28Ru is approximately 50% higher than that in Ni–18Ru, the differences in measured bulk conductivities are to be expected.

The values of contact resistance obtained from the heat-treated Ni–18Ru alloy after oxidation in air at 100 °C for up to 400 h are plotted in Fig. 6; values that were obtained previously for pure Cu and pure Ni under the same conditions are also shown on the figure for comparison. The heat-treated Ni–18Ru alloy displays excellent electrical contact properties with extremely low contact resistances even after 400-h exposure at 100 °C. The high contact resistance of pure Cu after oxidation for 400 h arises due to the formation of a relatively thick oxide scale (approximately 110 nm) consisting primarily of Cu_2O, a wide bandgap semiconductor ($E_g = 2.1$ eV) with poor bulk conductivity [16, 17]. The contact resistance of pure Ni is lower than that of Cu; this is mainly due to the formation of much thinner NiO scales [18], although here again the

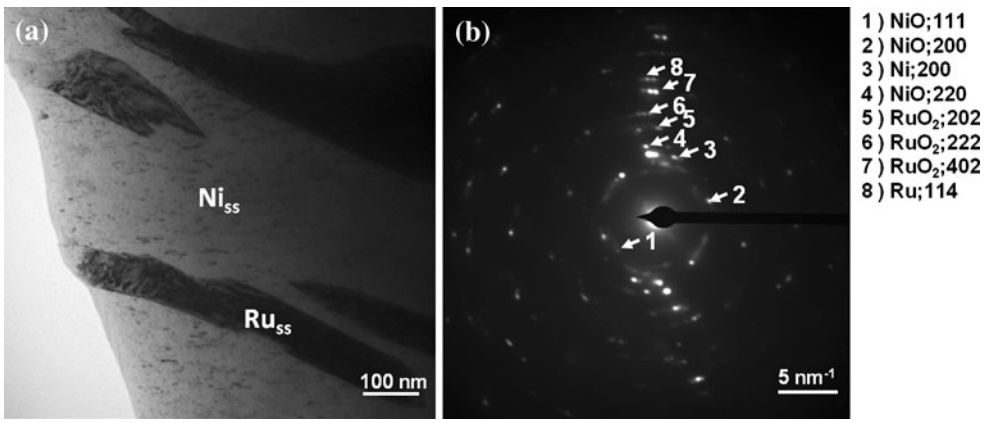

Fig. 5 TEM data obtained from a foil of the heat-treated Ni–18Ru alloy after oxidation for 40 h at 100 °C in air. **a** Representative bright field image of the β phase appears dark due to mass-thickness contrast, and the dimensions of the lamellae are consistent with the SEM observations (Fig. 4a). **b** SADP obtained from the region shown in Fig. 5a. The spacings of these spots indicate that four crystalline phases (α-Ni, β-Ru, NiO, and RuO_2) are present

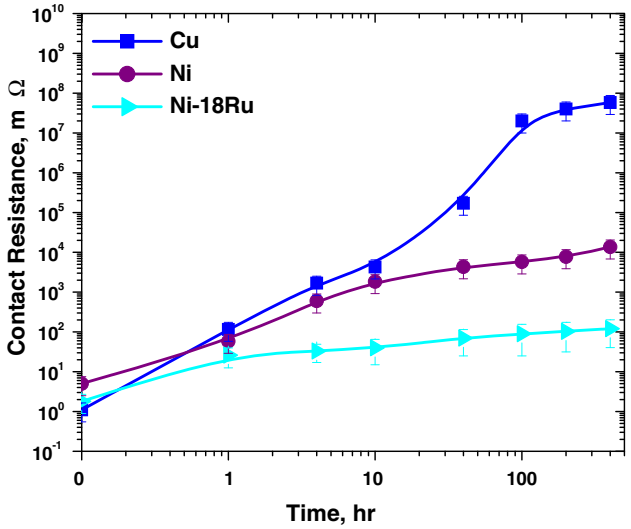

Fig. 6 Contact resistance of Ni–18Ru alloys oxidized at 100 °C in air as a function of oxidation time. Also shown are the contact resistance values obtained from pure Cu and pure Ni under the same conditions. The *error bars* are ±0.5 σ, where σ is the standard deviation of the measurements. The lines through the data are schematic trend lines drawn to help guide the eye

oxide is a wide-bandgap semiconductor ($E_g = 3.7$ eV) with relatively low bulk conductivity [16, 17]. The contact resistance of the Ni–18Ru alloy after 400 h was approximately six and two orders of magnitude lower than those of pure Cu and pure Ni after 400-h oxidation, respectively. The reasons for this are discussed below.

In an oxide scale comprising two distinct oxide phases, one with significantly higher bulk conductivity than the other, the contact resistance measured experimentally will depend on a variety of factors including the volume fractions of the two phases, the distributions of the phases; and the overall morphology/topography of the oxide scale. When such scales form on single-phase alloys, phase separation must occur within the oxide scale, and the higher conductivity oxide must form a percolative pathway between the underlying base metal and the scale surface to result in a decreased contact resistance. In cases where the underlying base metal is phase-separated, as in the case of Ni–Ru alloys, the situation is rather simpler. As discussed in the "Microstructures of the alloy and the oxide scale" Section, the microstructure of the Ni–18Ru alloy consists of lamellae of the Ni-rich α phase and the Ru-rich β phase. Upon oxidation, two distinct scales are formed: a NiO scale on the Ni-rich α lamellae, and a RuO_2 scale on the Ru-rich β lamellae. While stoichiometric NiO is an insulator, and oxygen-deficient NiO is a low-conductivity p-type semiconductor, RuO_2 is a 4*d*-oxide with metallic electrical conductivity (resistivity: 2×10^{-7} Ωm at 27°C, see [8] and references therein). The lower contact resistance measured for oxidized Ni–Ru alloys as compared with oxidized pure Ni can thus be ascribed to the formation of the metallic RuO_2 phase in the oxide scale that generates percolative pathways for sufficiently high Ru concentrations of the base alloy. The differences between the values of contact resistance obtained here for Ni–18Ru and those reported previously for Ni–28Ru are consistent with this since the latter alloy has a higher volume fraction of the Ru-rich β phase, and so a larger fraction of the contact area will consist of the conductive RuO_2 scale. We note that contacts produced from these alloys would have self-healing characteristics in situations where abrasive wear or fretting might occur since the oxide scale that would form on any re-exposed bare metal surfaces would again consist of the NiO–RuO_2 phase mixture.

Wear resistance

The measured values of mass loss during abrasive wear for the heat-treated Ni–18Ru alloy samples are plotted in Fig. 7 along with the corresponding values measured for pure Cu and pure Ni under the same conditions. The Ni–18Ru alloy displays excellent wear resistance with the mass loss at a sliding distance of 800 m being approximately 16 and 12 times less than those of pure Cu and pure Ni, respectively. All the three materials exhibit relatively fast wear mass loss in the initial 200-m "run-in" sliding distance, followed by a nearly linear variation of wear mass loss with sliding distance, in accordance with Archard's wear equation [19]. In SEM images obtained from the SiC paper after the completion of these wear tests (not shown here) it was observed

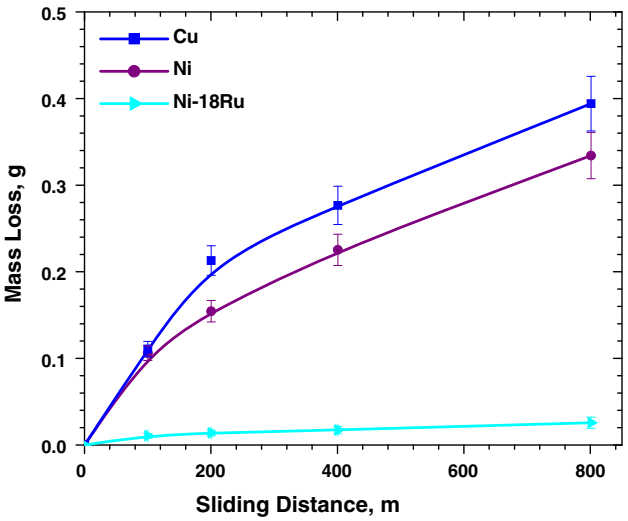

Fig. 7 Mass loss as a function of sliding distance for abrasive wear resistance tests on the heat-treated Ni–18Ru alloy using 5 N load. Also shown are the mass losses of pure Cu and pure Ni reference samples obtained under the same conditions. The *error bars* are ±0.5 σ, where σ is the standard deviation of the measurements. The *lines* through the data are schematic trend lines drawn to help guide the eye

that wear debris was trapped between the SiC particles with very little evidence of SiC particle debonding.

The excellent wear resistance of the Ni–18Ru alloy in comparison with the pure Cu and Ni can be attributed to the reinforcing effect of the hard lamellar Ru-rich β phase. Both Cu (38 HV) and Ni (65 HV) are much softer than Ru (410 HV). For Cu and Ni, two main material removal mechanisms operate during the wear process. First, the hard SiC can easily cut into the soft surfaces of Cu and Ni, causing the removal of large volumes of material. During sliding of the hard SiC against these soft metal surfaces, the frictional and shear forces result in deep micro-cutting/plowing, and evidence for this can be seen in Fig. 8a, b. Second, plastic deformation can lead to the accumulation of dislocations in the near surface regions, where these defects result in work hardening, and cracks could initiate. As described by Suh [20, 21], once formed these cracks can propagate leading to "delamination wear," and such delamination during sliding wear has been observed for a wide variety of different metallic systems (e.g., [22–26]). The observation of "flaked-off" regions in images such as Fig. 8a, b, and occasional flakes in the wear debris (not shown here), are evidence of this second mechanism. Although similar mechanisms can operate in the Ni–18Ru alloy, the extent of the wear is far less. This is mainly due to the higher hardness of the alloy: the mean value of hardness measured for the heat-treated Ni–18Ru alloy samples examined here was 360HV. The difference between this and the baseline value of 65HV for pure Ni is presumably due in part to the presence of the inherently harder β phase, and in part to the Hall–Petch and/or composite hardening of the α phase because of the lamellar microstructure. This is also reflected in the morphology of the worn surfaces as shown in Fig. 8c, d. These surfaces are much smoother than those of pure Cu and pure Ni: where micro-cutting/plowing grooves and flaked-off regions are observed, they are much shallower and narrower than those on pure Cu and Ni. This is consistent with the lower wear mass loss measured, as expected for a two-phase system wherein the phases have very different hardnesses (e.g., [22, 27–29]). We note that pure Ru is relatively brittle, and thus the Ni–Ru alloys with high β phase volume fractions might undergo other wear mechanisms involving brittle fracture. In the heat-treated Ni–18Ru alloy considered here, however, the β phase has a volume fraction of <20% and is present as thin lamellae in a more ductile α phase matrix. Thus, mechanisms requiring brittle fracture are unlikely to operate on a large scale.

Summary

We have studied the contact resistance and tribological properties of Ni–18Ru alloys. The alloys were fabricated

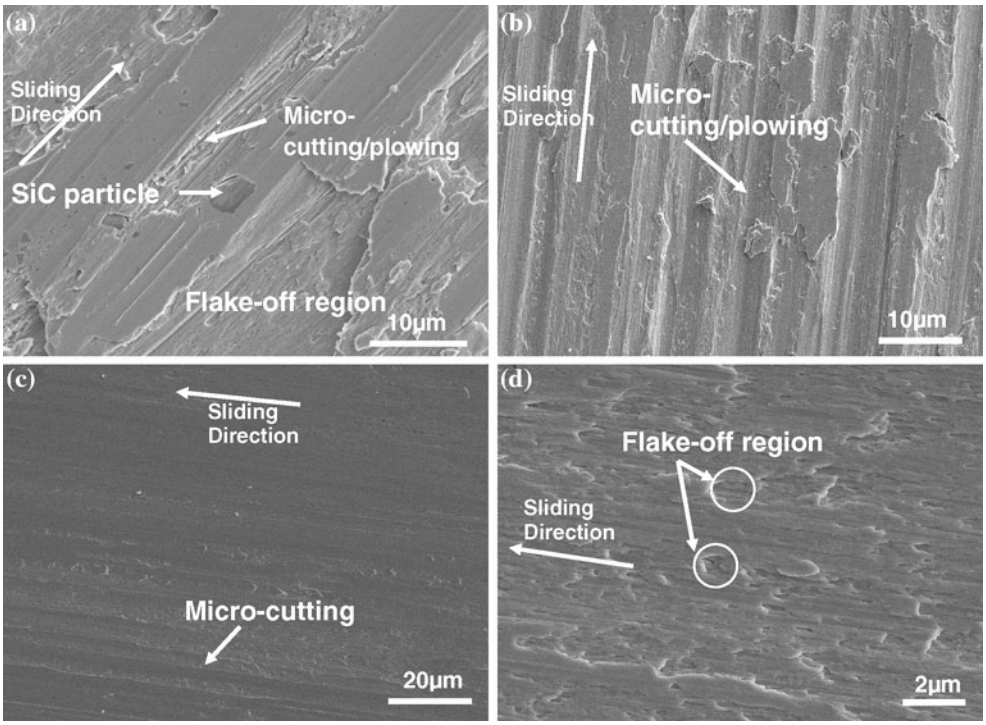

Fig. 8 SEM images showing the surface morphology of: **a** pure Cu, **b** pure Ni, and **c**, **d** the Ni–18Ru alloy after abrasive wear resistance tests under 5 N load for 800-m sliding distance

by arc-melting of elemental Ni and Ru followed by a homogenization treatment at 1100 °C and aging at 600 °C for 20 h. Our results show that

- The heat-treated Ni–18Ru alloys form a lamellar structure consisting of a Ni-rich α phase and a Ru-rich β phase.
- The oxide scale on this material replicates the lamellar structure of the underlying alloy and comprises cubic (NaCl-type) NiO and rutile RuO_2.
- The contact resistance of the alloy after 400-h oxidation at 100 °C is approximately six and two orders of magnitude lower than those of pure Cu and pure Ni after 400-h oxidation, respectively.
- The wear resistance of these alloys for a sliding distance of 800 m is approximately 16 and 12 times better than those of pure Cu and pure Ni, respectively.

These properties make the Ni–18Ru alloy a potential candidate for electrical contact applications. The combination of high wear resistance and the formation of a low-resistivity self-healing native oxide scale would be particularly attractive for sliding contacts, such as in switchgear. Moreover, such self-healing contact materials could also be exploited in a wide variety of other applications, such as fuel cells, high-temperature electronics, non-precious metal catalysts, photocatalytic hydrogen production, and solar cells.

Acknowledgements The authors gratefully acknowledge the support extended by the U. S. Army Research Office through Grant No. W-911-NF0710388.

References

1. Holm R (1967) Electric contacts: theory and applications. Springer-Verlag, Berlin
2. Slade PG (ed) (1999) Electrical contacts: principles and applications. CRC Press, Boca Raton
3. Braunovic M, Myshkin NK, Konchits VV (2006) Electrical contacts: fundamentals, applications and technology. CRC Press, Boca Raton
4. Antler M (1985) Wear 106:5–33
5. Beloufa A (2010) Tribol Int 43:2110–2119
6. Kim K (2010) Wear 269:655–663
7. Aindow M, Alpay SP, Liu Y, Mantese JV, Senturk BS (2010) Appl Phys Lett 97:152103
8. Tsuda N, Nasu K, Fujimori A, Siratori K (2000) Electronic conduction in oxides, 2nd edn. Springer, New York
9. Keith MG, James RC (1993) Phys Rev B 47:1732
10. Mattheiss LF (1976) Phys Rev B 13:2433
11. Graebner JE, Greiner ES, Ryden WD (1976) Phys Rev B 13:2426
12. Boshta M, Gad SA, El-Soud AMA, Mostafaa MZ (2009) J Ovonic Res 5:1–8
13. Jang WL, Lu YM, Hwang WS, Chen WC (2010) J Eur Ceram Soc 30:503–508
14. Hakim A, Hossain J, Khan KA (2009) Renew Energ 34: 2625–2629
15. ASTM Standard B 667-97, Standard Practice for Construction and Use of a Probe for Measuring Electrical Contact Resistance, 1997
16. Tamai T (1989) Electron Commun Jpn Part 2. Electron 72:87–93
17. Zhu YF, Mimira K, Lim J, Isshiki M, Jiang Q (2006) Met Mater Trans A 37A:1231–1237
18. Veeka Kumari S, Natarajan M, Vaidyan VK (1992) J Mater Sci Lett 11:761–762
19. Chang C, Wang C, Jin Y (2010) Wear 29:167–173
20. Suh NP (1973) Wear 25:111–124
21. Suh NP (1977) Wear 44:1–15
22. Gui MC, Kang SB, Lee JM (2000) J Mater Sci 35:4749–4762
23. Gialanella S, Ischia G, Straffelini G (2008) J Mater Sci 43:1701–1710
24. Al-Qutub AM, Allam IM, Samad MAA (2008) J Mater Sci 43:5797–5803
25. Kumari UR, Rao PP (2009) J Mater Sci 44:1082–1093
26. Zhao YT, Wang SQ, Yang ZR, Wei MX (2010) J Mater Sci 45:227–232
27. Savaskan T, Bican O, Alemdag Y (2009) J Mater Sci 44: 1969–1976
28. Srivastava VC, Rudrakshi GB, Uhlenwinkel V, Ojha SN (2009) J Mater Sci 44:2288–2299
29. Yan SQ, Xie JP, Liu ZX, Li JW, Wang WY, Wang AQ (2009) J Mater Sci 44:4169–4173